ACS ENVIRONMENTAL Au
AN OPEN ACCESS JOURNAL OF THE AMERICAN CHEMICAL SOCIETY

pubs.acs.org/environau
Article

Self-Cross-Linking of MXene-Intercalated Graphene Oxide Membranes with Antiswelling Properties for Dye and Salt Rejection

Saurabh Kr Tiwary, Maninderjeet Singh, Farzana Hasan Likhi, Siddharaj Dabade, Jack F. Douglas, and Alamgir Karim*

Cite This: ACS Environ. Au 2024, 4, 69–79
Read Online

ABSTRACT: Membrane-based water purification is poised to play an important role in tackling the potable water crisis for safe and clean water access for the general population. Several studies have focused on near two-dimensional membranes for this purpose, which is based on an ion rejection technique. However, membrane swelling in these materials has emerged as a significant challenge because it leads to the loss of function. Herein, we report a self-cross-linked MXene-intercalated graphene oxide (GO) membrane that retains ion and dye rejection properties because the physical cross-linking interaction between Ti−O−Ti and neighboring nanosheets effectively suppresses the swelling of the membrane. In addition to the associative Ti−O−Ti bonds, C−O−C, O═C−O, and C−OH bonds are also formed, which are important for inhibiting the swelling of the membrane. To ensure the longevity of these membranes in a service context, they were subjected to heat pressurization and subsequent thermal annealing. The membrane subjected to this novel processing history exhibits minimal swelling upon immersion in solutions and retains function, rejecting salt and dyes over a wide range of salt and dye concentrations. Furthermore, these membranes successfully rejected dye and salt over a period of 72 h without a degradation of function, suggesting that these membranes have the requisite durability for water filtration applications.

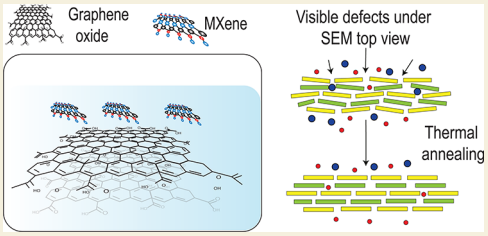

KEYWORDS: *membrane separation, two-dimensional polymers, graphene oxide MXene membranes, physical cross-linking, ion sieving, swelling inhibition, mechanical compression*

INTRODUCTION

Despite the abundance of water on earth, a significant portion of the world's population is facing the possibility of losing access to clean water.[1−3] To address this socially important issue, scientists have proposed the use of membrane-based technologies, like reverse osmosis (RO) membranes, to remove salt from water belonging to various sources, including brackish groundwater, recycled wastewater, seawater, and other environmental remediation contexts.[4] Although RO technology approaches the theoretical minimum energy required for saltwater separation, RO systems continue to carry significant costs. Enhancing system efficiency can then be achieved through process intensification.[5] Thus, two-dimensional graphene oxide (GO)-based membranes show great promise in water and wastewater treatment for their high flux and, thus, potential for intensifying the desalination process and improving its system efficiency.

GO sheets, which are made from graphite and disperse easily in water due to their ionized oxygen groups, have been found to form paper-like membranes with exceptional mechanical properties.[6] Although GO films are known for their stability in water, their negative charge would typically cause them to separate from each other.[7] There have been reports of GO films redispersing in water,[8] highlighting the need to ensure their structural integrity. Due to unresolved issues pertinent to swelling, employing these near two-dimensional membranes for ion rejection has emerged as a major problem.[9] Upon immersion in aqueous solutions, it has been found that these membranes tend to exhibit significant water absorption into the space between the layers of neighboring sheets, and owing to this phenomenon, the membranes swell significantly, and their ion-exclusion capacity is degraded.[10] In some instances, the GO's interlayer spacing has even increased by a factor of 2 under aqueous conditions compared to the dry material. There is a practical "molecular permeation cutoff" near ≈1.0 nm that implies that smaller hydrated salt ions, such as Na^+ (0.70 nm), Cl^- (0.66 nm), and SO_4^{2-} (0.76 nm), then exhibit low rejections.

Recent developments have focused on enhancing the efficiency and stability of these membranes.[11,12] For instance, a study demonstrated that the cross-linking of divalent cations could improve resistance against swelling in partially reduced GO membranes, leading to improved dye-rejection efficiencies

Received: September 22, 2023
Revised: November 22, 2023
Accepted: November 28, 2023
Published: January 8, 2024

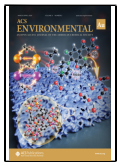

https://doi.org/10.1021/acsenvironau.3c00059
ACS Environ. Au 2024, 4, 69–79

Scheme 1. Schematic of the Dynamically Cross-Linked GO/Mxene Membrane for Dye and Salt Rejection Applications

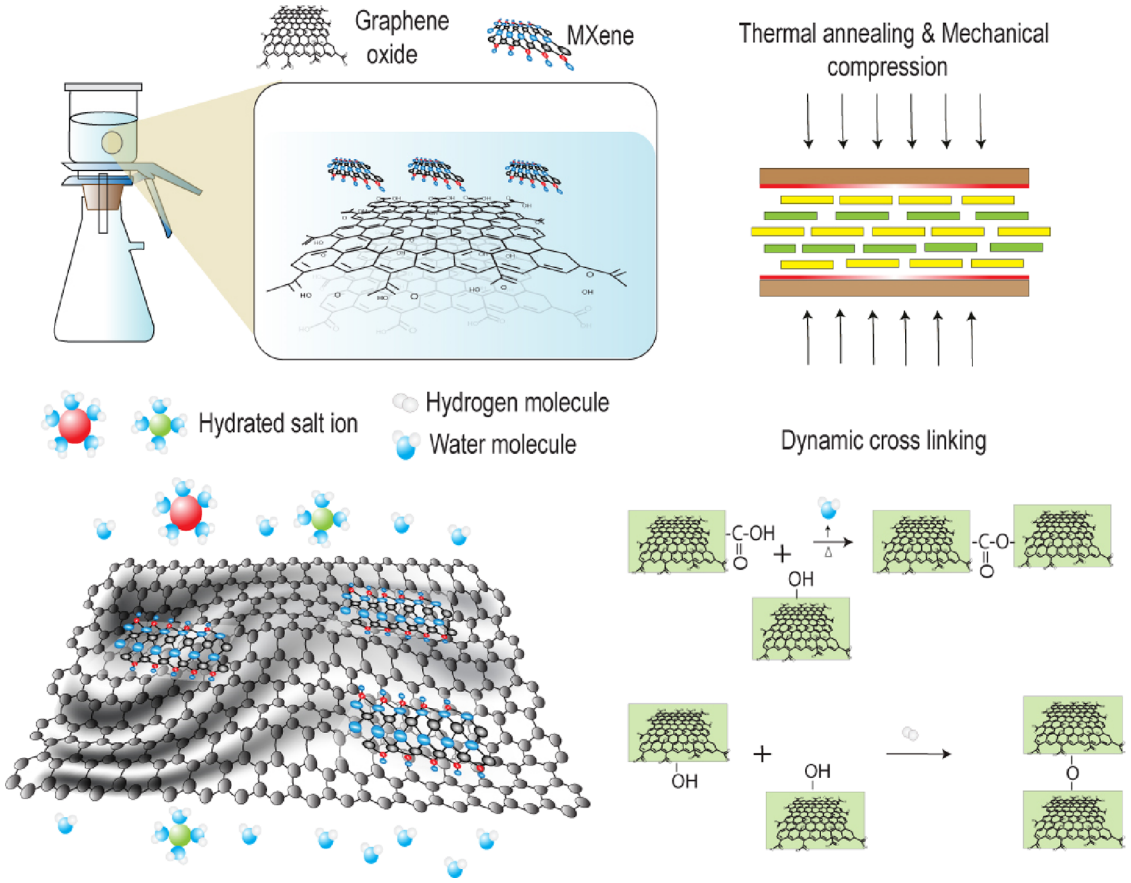

of up to 98.88% for certain dyes.[13] In another research by Chandio et al.,[14] a GO membrane was fabricated by employing a cross-linker, which was chosen to be serine amino acid (SAA), and reducing agent. The fabricated membrane showed impressive results by appreciably rejecting dyes like rhodamine B and methyl blue and salts like NaCl, $MgCl_2$, and $Pb(NO_3)_2$ while maintaining ultrafast permeability. In addition to the impressive rejection performance, the membrane also remained stable for several days in an aqueous milieu. There remain several challenges associated with the GO-based membranes proposed in the literature, with the primary one being associated with the inability to control the interlayer spacing. The variation of interlayer spacing between the GO sheets makes it difficult to reduce the interlayer spacing sufficiently to exclude small ions and to maintain this spacing against the tendency of GO membranes to swell in an aqueous environment.[15]

Wang et al.[5] suggested that microstructural control of these membranes might be achieved through the introduction of strong $\pi-\pi$electrostatic interaction between GO and π-conjugated polycyclic cations[16] that might inhibit the membrane swelling. It was admitted in this work, however, that the noncovalent nature of these interactions might make these materials unstable under solutions and thus unsuitable for commercial applications.[17,18] The present work explores a new noncovalent cross-linking strategy for stabilizing this class of membranes.

MXenes[16] are two-dimensional (2D) metallic materials composed of transition metal carbides and nitrides.[6,19,20] The MXene family involves the addition of various hydrophilic $Ti_3C_2T_x$ functional groups (T corresponds to hydroxyl, oxygen, or fluorine groups), and this material has proven to be chemically versatile and useful in numerous previous applications.[21] In particular, there are many applications in the areas of energy storage, electromagnetic interference shielding,[22,23] membrane-based separation, and other areas, and these materials continue to be of great interest for many applications.[24,25] MXene exhibits superior resistance to swelling compared to GO. When MXene, specifically $Ti_3C_2T_x$, is combined with graphene, it readily integrates into the graphene sheet layers. Moreover, the nanosheet surface of MXene is rich in surface functional groups, such as oxygen (O), hydroxyl (−OH), and fluorine (−F), which are anticipated to interact with the carboxyl and hydroxyl groups of GO. Consequently, the swelling behavior of GO-MXene membranes is inhibited, which is advantageous for their ability to effectively block metal ions.

The strong cross-linking between MXene and graphene ensures robust adhesion and long-term stability of the membrane, resulting in extensive graphene coverage. Additionally, this minimizes the likelihood of positional deviations of the intercalating agent, facilitating the scalability in the development of these membranes.

Starting from this class of materials, we developed a novel GO-MXene material specifically for water purification applications. The key idea, noted above, is to stabilize the material against swelling and loss of function in salt rejection through the introduction of covalent cross-links between MXene−MXene, GO−GO, and MXene−GO interlayers. This particular approach has several advantages, such as the

https://doi.org/10.1021/acsenvironau.3c00059
ACS Environ. Au 2024, 4, 69−79

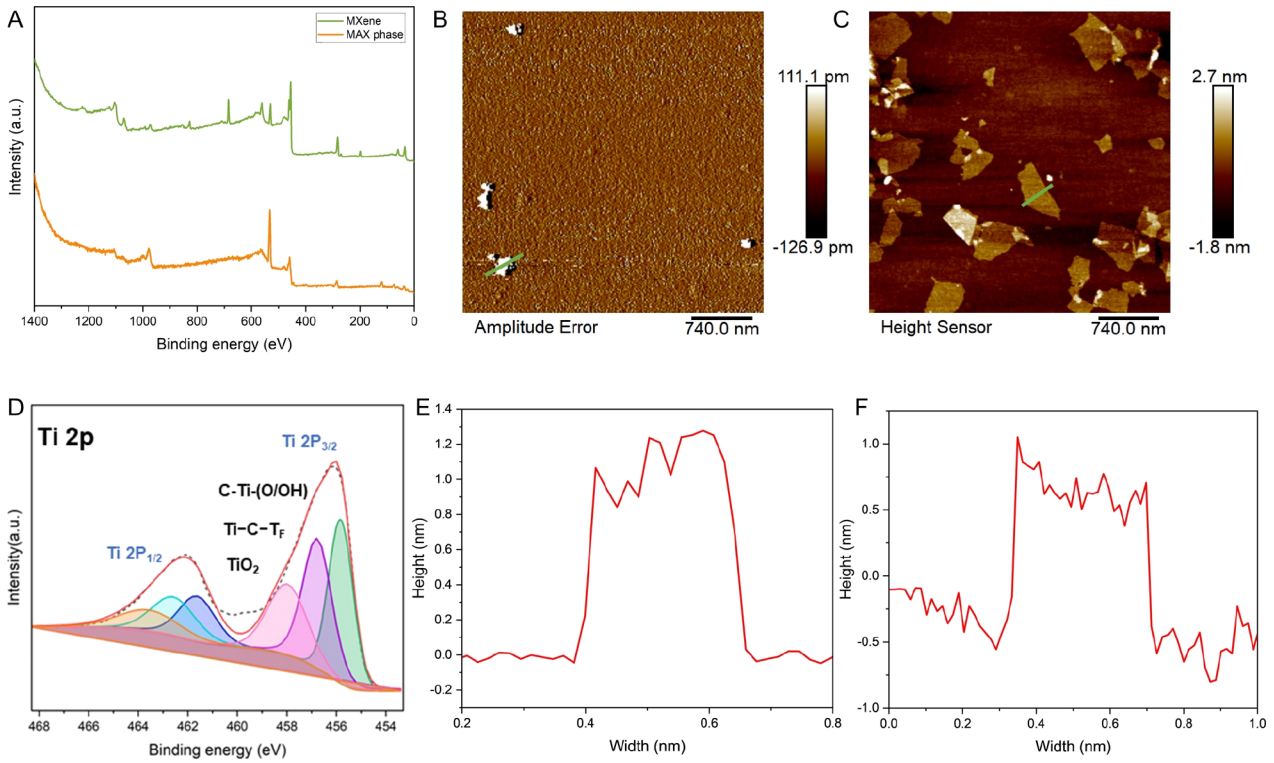

Figure 1. (A) XPS survey scan spectrum of the MXene and MAX phase. (B) AFM image of the MXene nanosheet on a silicon wafer. (C) AFM image of the GO nanosheet on a silicon wafer. (D) Component peak fitting of the XPS spectrum for Ti 2p. (E) Height profile of MXene. (F) Height profile of the GO nanosheet.

hydrophilic nature of GO, which increases the membrane's hydrophilicity, and the small pore size of MXene, which can effectively remove most salts and contaminants. An interesting possibility is that the MXene's intercalation into the GO membranes might also assist the rejection of salt ions because the highly hydrated salt ions cannot easily pass through the interlayer spaces. To further restrict the size of 2D sheet interlayer spacing and improve ion rejection, the GO-MXene membrane was mechanically compressed using heated plates to reduce the interlayer *d*-spacing and finally thermally annealed under a vacuum. This combination of mechanical compression and annealing led to a significant improvement in salt rejection of the membrane. We find that these processed near 2D membranes have adjustable molecule/ion sieving capability, good thermostability up to 120 °C, easy preparation, and good antiswelling properties. Here, MXene works as an intercalant between GO membranes that significantly enhances the composite membrane's monovalent ion rejection and dye rejection properties. The salt rejection mechanism here involves the transport of water and salt through the interlayer spacing that exists between the stacked 2D sheets. This interlayer spacing can be adjusted to allow the passage of water while rejecting larger hydrated ions by size exclusion.

To create the 2D lamellar composite membrane that could resist swelling, utilizing both MXene and GO, we employed a self-cross-linking approach. It is necessary to note that there is a formation of cross-links between adjacent GO−GO and MXene−MXene nanosheets. These cross-links are termed "self-cross-links", and in the case of GO sheets, there can be covalent self-cross-linking.[26]

Herein, both MXene and GO contain numerous surface functional groups (−O, −OH, −F, and −COOH) with pliable and hydrophilic surfaces. Thus, through self-cross-linking, we infused these surface functionalities with each other, thereby creating a stable covalent bond.[26,27] This design approach enables us to limit the interlayer spacing and inhibit membrane swelling within the GO-MXene composite membrane. These channels facilitate the transportation and segregation of water molecules, leading to efficient water purification performance, as demonstrated in Scheme 1.

EXPERIMENTAL SECTION

Synthesis and Characterization of MXene Powder

The etching of Ti_3AlC_2 powder leads to the formation of MXene ($Ti_3C_2T_x$) powder, and in this study, it was done by first dissolving 2.0 g of lithium fluoride (LiF, 98+%, Alfa Aesar) in 20 mL of 9 M hydrochloric acid (diluted from concentrated HCl, 48−51%, Sigma-Aldrich) solution. The dissolution took place with continuous stirring. Next, to prevent overheating, 2.0 g of Ti_3AlC_2 powder was added to the resulting solution over approximately 10 min, and the resultant solution underwent stirring for 24 h at 62.83 rad/s and 35 °C. Following rigorous stirring, the next step was that of acid removal. For this, deionized (DI) water (100 mL) was mixed in the stirred solution and centrifuged for 5 min at 366.51 rad/s for 5 min, following which the supernatant was decanted. This washing step was repeated until the supernatant's pH converged to 6. Finally, a solid residue was obtained and then subjected to vacuum filtration, and drying under a vacuum led to the formation of $Ti_3C_2T_x$ powder. Moreover, the powdered MXene was mixed in DI water followed by sonication for 4 h to reduce the flake size of MXene nanosheets, as shown in Figure 1E. Using the AFM image (Figure 1B) and height profile of MXene (Figure 1E), it has been shown that the average thickness of the MXene nanosheets is about ∼1.1 nm. Figure S3A depicts the size distribution of the MXene nanosheet, and Figure S2 and Figure 1A

https://doi.org/10.1021/acsenvironau.3c00059
ACS Environ. Au 2024, 4, 69−79

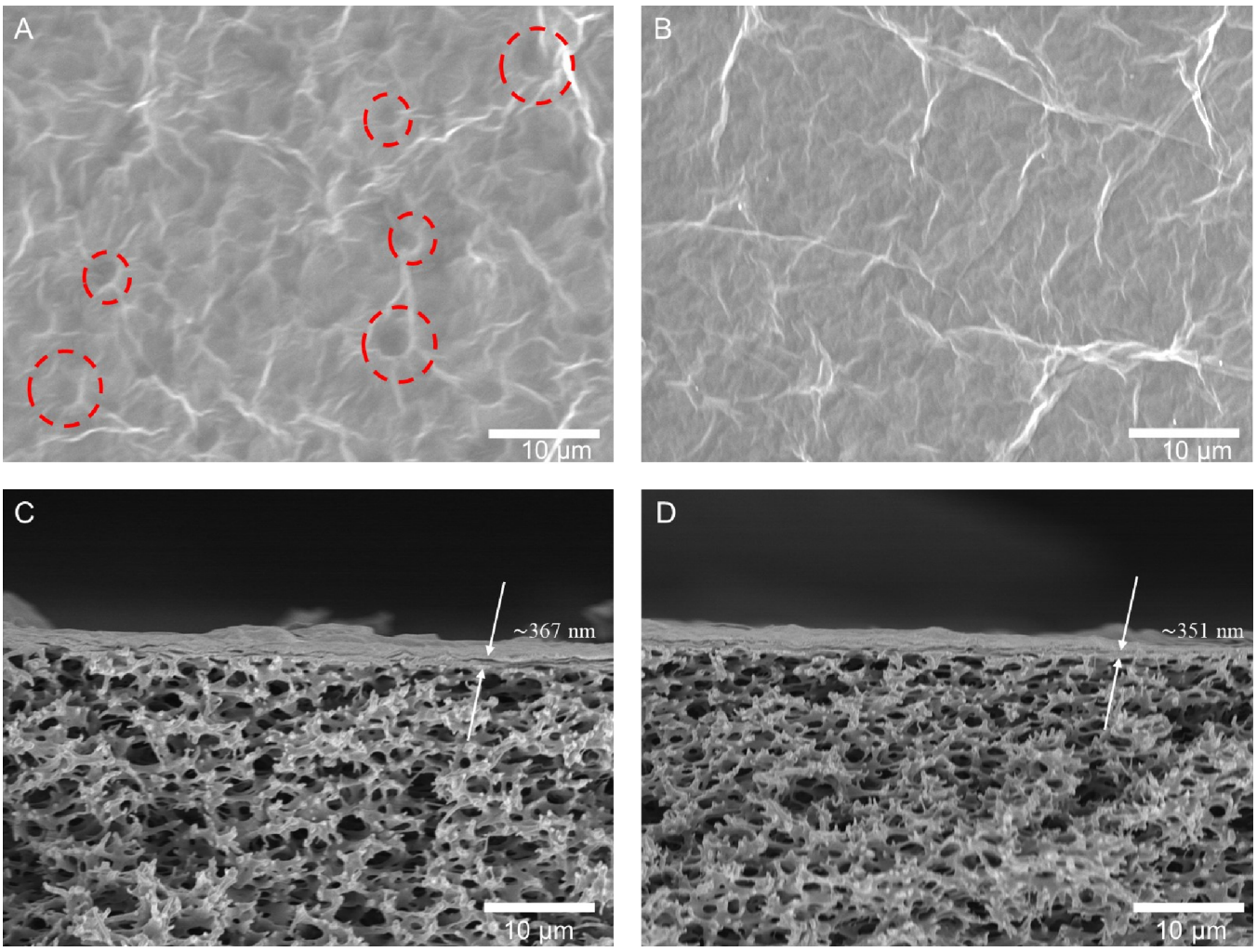

Figure 2. SEM top-view microstructure images of (a) GO-MXene and (b) m-v120-GO-MXene PES-supported membranes. (c) Cross-sectional SEM images of (c) GO-MXene and (d) m-v-120-GO-MXene PES-supported membranes.

shows the XRD and XPS spectra of MXene, respectively. As can be seen in Figure 1A, there are peaks at binding energy values that are close to ~300, 430, and 460 eV, which correspond to C 1s, Ti 2p, and O 1s, respectively.[28] In Figure 1D, the component peak fitting of the XPS spectrum for C 1s shows that the MAX phase has been successfully exfoliated to the MXene nanosheets.[16]

Preparation of MXene-GO Membranes

Graphene oxide solution was purchased from Graphene Supermarket with an initial concentration of 6.2 g/L. To prepare a 2 g/L solution of GO (reagent X), DI water was used, and the solution was vigorously stirred for a minimum of 10 min followed by 30 min of ultrasonication. Next, 1 g/L of MXene (reagent Y) was dissolved in DI water. A small volume (100 μL) of the reagent Y solution was then added to 100 mL of DI water, and the mixture was stirred vigorously for 10 min. These solutions were then combined with reagent X (600 μL) while being stirred vigorously to obtain GO-MXene dispersions. Here, to inhibit the infiltration of target ions through indiscriminate channels, GO was added to $Ti_3C_2T_x$. The interedge defects or pinholes in the composite membranes served as indiscriminate channels. The aqueous dispersions of both substances were passed through permeable 100 nm pore size polymeric supports, PES (poly(ether sulfone), to prepare GO-MXene composite membranes. These dispersions were vacuum filtered through a 200 nm pore size PES support with a 2 in. diameter under a vacuum pressure of −40 kPa (−300 mmHg) to obtain GO-MXene membranes. To ensure no disturbances due to the flow of air, a stainless steel cover was placed on top of the filtration, which was removed once filtration was completed. Also, the GO-MXene membranes were kept for at least 5 h under vacuum conditions. Finally, the membranes were removed (shown in Figure S1) and left to dry for at least 24 h at room temperature, and last, to obtain self-cross-linked membranes, they were subjected to heating under vacuum conditions at 120 °C for 24 h. The resultant self-cross-linked membrane was taken for characterization, and their permeation measurements were carried out. Using the AFM image (Figure 1C) and height profile of the GO nanosheet (Figure 1F), it was shown that the average thickness of GO nanosheets is ~1 + 0.12 nm. Also, Figure S3B depicts the size distribution of the GO nanosheet.

Characterization

The Thermo-Fisher Scientific Axia ChemiSEM was used to capture SEM images. XRD analysis was carried out on a Bruker D8 Advance apparatus using filtered Cu Kα radiation, with a step size of 0.02° and a step time of 2 s, in the range of 2−10° or 2−90°. The Thermo-Scientific Nicolet IS5 unit was used for FTIR characterization in the wavenumber range of 500−4000 cm^{-1}. An ESCALAB 250 spectrometer from Thermo-Fisher Scientific was used for XPS analysis with monochromatic Al Kα radiation (1486.6 eV) at a pressure of 2.66×10^{-7} Pa. The Bruker MultiMode 8 scanning probe microscope (SPM, VEECO) was used to obtain AFM images in tapping mode. For roughness measurement of the membrane surface, atomic force microscopy (AFM) analysis (DMFASTSCAN-SYS, Bruker, Germany) was carried out, with the scanned area being 3 × 3 μm. The Ramé−Hart Contact Angle Goniometer was used to measure the water contact angle. The Thermo-Scientific Evolution

https://doi.org/10.1021/acsenvironau.3c00059
ACS Environ. Au 2024, 4, 69−79

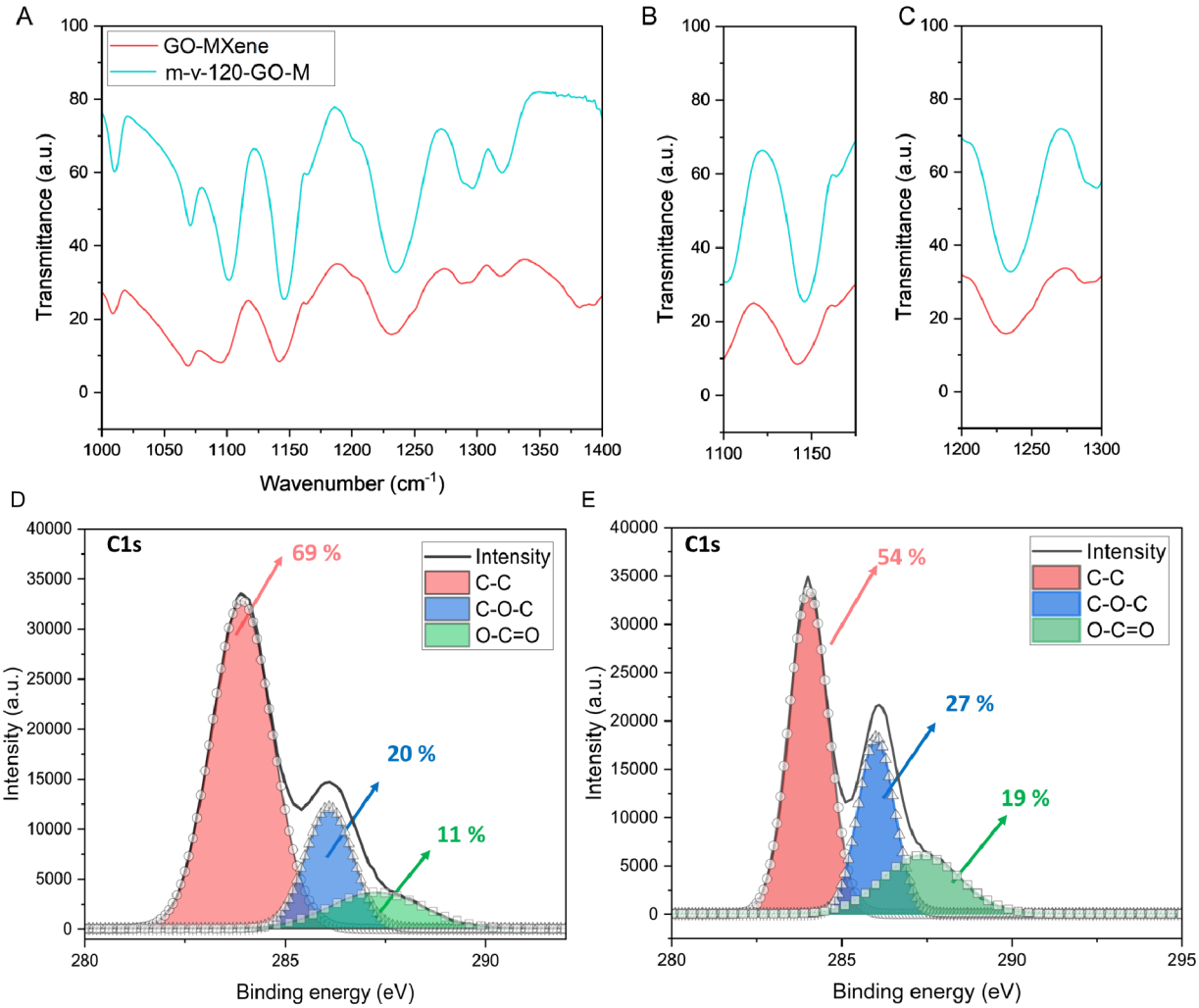

Figure 3. (A–C) FTIR spectra of GO-MXene and m-v-120-GO-MXene. Component peak fitting of the XPS spectra for C 1s for (D) GO-MXene and (E) m-v-120-GO-MXene.

201 UV–vis (ultraviolet–visible) spectrophotometer was used to measure the absorbance spectra of the organics used. The SevenCompact Duo pH/conductivity meter was used to measure the permeate conductivity.

Ion Permeation Measurement

The dead-end cell mode of operation was utilized to conduct water lux and salt (NaCl and $MgCl_2$: 0.5–5 g/L) rejection tests on the membranes.[16] The nitrogen line was adjusted to control the operating pressure within the range of 0–2 bar, as measured by an equipment with an accuracy of 0.2 bar. The membrane had a diameter of 1 in., and the measurements were taken at room temperature.

To measure the flux of salt, the permeation of a salt solution with a specific concentration was done across the membrane at a pressure of 1 bar for a minimum of 40 min to achieve a steady test state. Following this, to ensure data accuracy, the data were collected at 2.0 bar every 10 min for a minimum of 2 h. To ensure the reliability of our results, we tested each type of membrane at least five times using five replicated membranes. The salt permeance was then determined using the relation

$$\text{permeance} = \frac{\text{volume of permeate obtained (L)}}{\text{membrane area (m}^2\text{)} \times \text{pressure difference (bar)} \times \text{time (h)}} \quad (1)$$

An ion-conductivity meter (RS485, Mettler Toledo) was utilized to measure the ionic conductivity of the feed, permeate, and retentate. The rejection rates were determined using the following formula:

$$\text{rejection (\%)} = \left(1 - \frac{C_p}{C_f}\right) \times 100 \quad (2)$$

where C_p and C_f represent the concentration of permeate and feed solutions.

To prevent concentration polarization or molecular adsorption during prolonged dead-end filtration, we collected permeate solutions weighing 5 g on average for each time interval.

Preparation of Mechanically and Thermally Treated Composite Membrane

The GO-MXene (GO-M) composite membranes were created by following two methods: mechanical compression and thermal compression/annealing. The thermal annealing of GO-M was performed in a vacuum drying chamber for 24 h at temperatures of 120 °C, resulting in a membrane called v-GO-M (vacuum GO membrane). For mechanical compression, the vacuum annealed GO membrane (v-GO-M) was put in between a dual heat press machine for 300 s at 80 °C (m-v-120-GO-M) (mechanically compressed vacuum annealed GO membrane). Then, the membranes were cooled to room temperature and used for permeation measurements.

https://doi.org/10.1021/acsenvironau.3c00059
ACS Environ. Au 2024, 4, 69–79

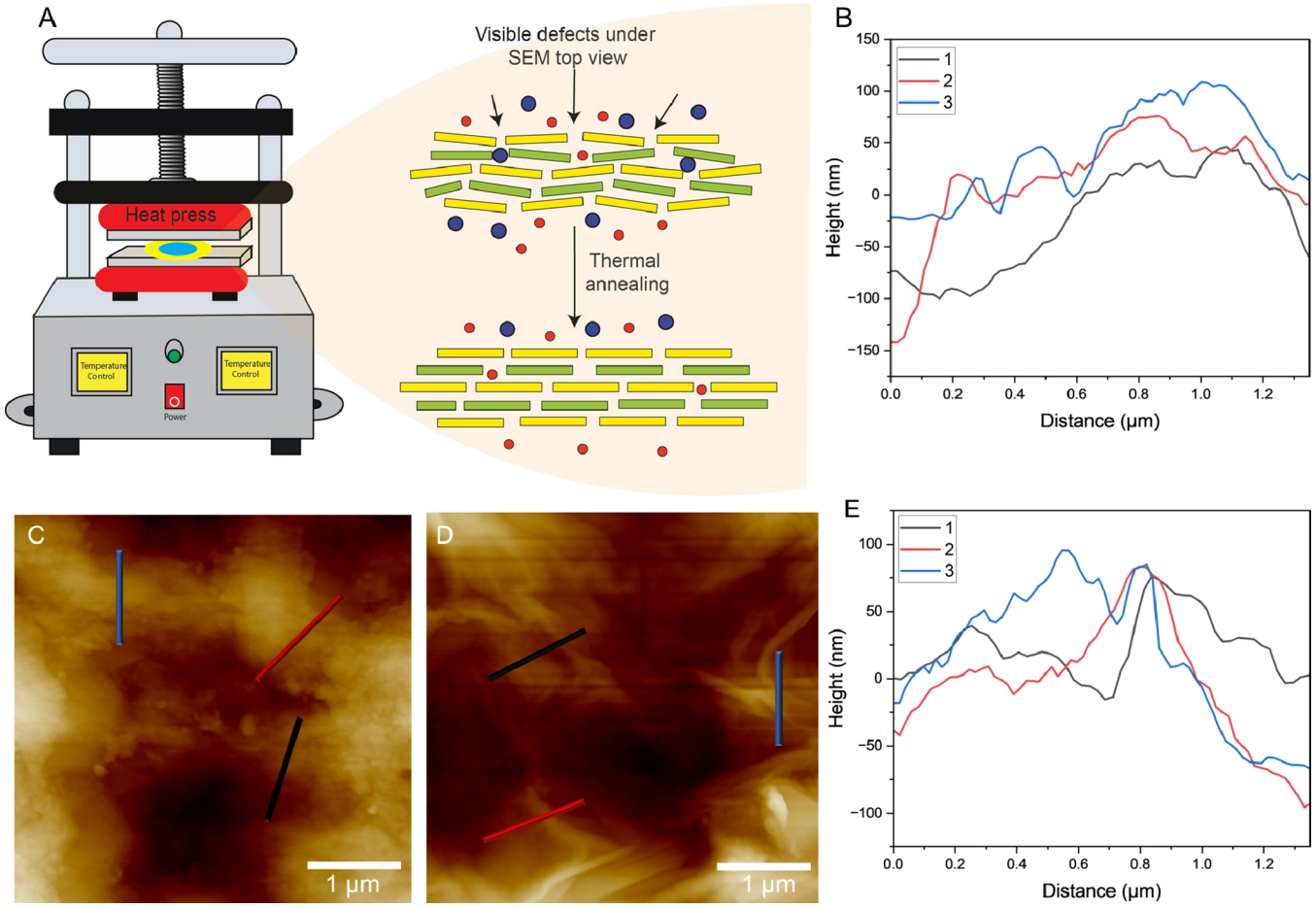

Figure 4. (A) Heated press that enhances the uniformity of the membrane flakes. (B) Height distribution of the membrane shown in panel C. (C) AFM image of the membrane after going through the heat press and being used for desalination. (D) AFM image of the membrane that is mechanically pressed and thermally annealed. (E) Height distribution of the membrane shown in panel D.

RESULTS AND DISCUSSION

Figure 2A–D displays the top and cross-sectional view of the GO-MXene composite membrane on poly(ether sulfone) (PES) via SEM images. In Figure S4, the PES alone cross-sectional SEM image shows the bulk phase PES microstructure. The top-view SEM image of the GO-MXene membrane illustrates that the surface of the GO-MXene composite membrane has small holes distributed uniformly over the surface, as shown in Figure 2A. Holes were clearly visible on the membrane surface even at 30 μm magnification under the SEM images (shown in Figure S5). However, this holelike structure disappears after mechanical compression and thermal annealing at 120 °C due to pore shrinkage (Figure 2B and Figure S6). This is again a clear indication of the occurrence of cross-linking in the membrane. Figure 2B also depicts wrinkles, and their presence is credited to the stacking of the GO boundaries.[29,30] Also, the cross-sectional SEM images (Figure 2C,D and Figure S7) demonstrate the reduction in membrane thickness after mechanical compression and thermal annealing. For GO-M (Figure 2A) and m-v-120-GO-M (Figure 2B), the membrane thickness was ~367 and ~351 nm, respectively.

The fabrication of GO-M and m-v-120-GO-M membranes was achieved via reactions between adjacent MXene and GO nanosheets that include the following functional groups: −COOH and −COOH, −COOH and −OH, and − OH and −OH, as shown in Scheme 1. Fourier-transform infrared spectroscopy (FTIR) was performed to probe changes in the functional groups on GO-M after mechanical compression and thermal annealing. The transmittance spectra were taken for several GO films, each with at least three spots, all of which yielded similar results, as shown in Figure 3A with the two FTIR spectra of GO-M and m-v-120.[24,25,31,32]

There were several ubiquitous specialties in the GO-MXene embrane (Figure S8), specifically the appearance of absorption associated with water (~3000 and 1600 cm^{-1}) after processing, whereas the broadest differences exist at values close to 1225 cm^{-1} (Figure 3B) and 1140 cm^{-1} (Figure 3C). When the FTIR spectrum, which corresponds to Figure S9, of GO-M was compared to m-v-120-GO-M, peaks were observed at ~730 and ~850 cm^{-1}, and these are credited to the stretching vibrations of the Ti−O−Ti bond. Primarily, these differences are a result of vibrations that take place in ester bonds given the dehydration reactions. There are minimal variations between both the aforementioned samples; however, when differences in spectroscopical values were observed for GO-MXene from distinct samples, a similarity in trend was observed. A relative increment in intensity was observed at 1140 cm^{-1}, whereas after mechanical compression and thermal annealing were performed, a new and small peak was seen at 1225 cm^{-1}, which is because new bonds of C−O−C are formed. Given the formation of an ester bond with the GO surface, we report that enhanced signal intensities are found at

https://doi.org/10.1021/acsenvironau.3c00059
ACS Environ. Au 2024, 4, 69−79

values ranging between 1350 and 1000 cm^{-1}. The presence of a hydroxyl group on the surfaces of MXene and GO nanosheets led to the formation of Ti−O−Ti bonds, Ti−O−C bonds, and O═C−O and C−O−C bonds via dehydroxylation between neighboring GO-MXene nanosheets. The chemical composition of carbon in the GO-M was analyzed by using surface-sensitive X-ray photoelectron spectroscopy (XPS). The results, depicted in Figure 3D,E, provide insights into the elemental state within the membranes. In Figure 3D, the C 1s region of GO-M demonstrates that the carbon is present in three different forms: C−O−C constitutes 20% of the carbon content, O−C═O makes up 11%, and C−C accounts for 69%. Following the thermal self-cross-linking process, changes in the carbon composition are observed in m-v-120-GO-M. Figure 3E reveals that the fraction of C−C decreases to 54% after the process. Simultaneously, the fractions of C−O−C and O−C═O increase to 27 and 19%, respectively. These findings suggest that the thermal self-cross-linking and cross-linking process alters the distribution of carbon moieties within m-v-120-GO-M compared to the original GO-M. The analysis of the O 1s region in GO-M (Figure S10A) demonstrated that the C−Ti−O_x fraction accounted for 91% of the composition, whereas the C−Ti−$(OH)_x$ fraction constituted 9%. Following the thermal self-cross-linking process, the C−Ti−O_x fraction increased to 94%, whereas the C−Ti−$(OH)_x$ fraction decreased to 6% (Figure S10B). This shift indicates a conversion from −OH groups to −O− groups, implying the transformation of −OH to −O− through the reaction −OH + −OH = −O− + H_2O during the thermal treatment.

In summary, the surface view of m-v-120-GO-M further reveals a dense coverage without any visible defects, as observed before membrane treatment (shown by dashed circles in Figure 2a) (Figure 4E). As found previously in Figure 2A,B, wrinkles[33] are observed in these AFM images as well (Figure 4D).

To illustrate the superior molecular separation abilities of these composite GO membranes, we next assessed the rejection efficiency of the composite membrane against those of the GO stand-alone membranes using eq 2. It was found that the cross-linked membranes displayed superior rejection than GO-M and mechanically compressed GO-M. The membranes under consideration can only tolerate low bands of pressure, which result in low permeance, because of which the amount of time that the membrane needs to be properly functional increases. In the case of the cross-linked membranes, the observed rejection rates after 48 h dropped by 10% for NaCl and 7% for $MgCl_2$, and these reductions limit the utility of cross-linked membranes.

The SEM images display visible impressions of pores (Figure 2A), whereas the AFM images reveal depressed areas measuring approximately 150 nm in height (Figure 4B,E), confirming the existence of semifree swelling basin structures. The AFM measurements also confirm the reduction in the surface roughness parameters of the membrane due to mechanical compression and thermal annealing. Figure S11 shows the AFM image of a thermally annealed GO-MXene membrane after 48 h of permeation measurement, demonstrating a significant roughness change. The characterization of the surface morphology of the membranes, with the roughness of the membrane surface is reflected by the bright and dark shades in the AFM images.[34−37] The roughness parameters are listed in Table 1. These observations demonstrate that subtle compaction effects that could be taking place, such as migration and rearrangement, and cross-linking of the GO-MXene flakes occurs during the thermal annealing process. Furthermore, it is possible that the annealing process increases the adhesive forces between the GO-MXene layer through mechanisms that are not fully understood yet. In short, our observations show the replacement of the deep valleys in the GO-M by many small peaks in the compressed and annealed GO-MXene membrane, whereas it had a smoother surface than the GO-MXene membranes due to hydrophilic GO being cross-linked with MXene under a vacuum, and the results also suggest that the modification of the GO membrane with MXene can reduce the surface roughness of the GO membrane. The mechanically compressed and thermally annealed membrane's roughness parameters were calculated for two different cases. The first is the case where it was directly employed after preparation (Figure 4D), and the second is the case where the parameters were calculated for the membrane used (Figure 4C). When both of these cases were compared for the mechanically compressed and thermally annealed membrane, a decrement in the roughness parameters was observed (Table 1).

Table 1. Surface Roughness Parameters Derived from AFM for the GO-MXene Membrane

membrane	Rq (nm)	Ra (nm)
m-v-120-GOM	130	106
m-v-120-GOM-used	116	96

The GO-MXene membrane was compressed mechanically under external pressure, with the temperature of the pressing plates being 79.85 °C and the process of thermal annealing being the same as before. Owing to this modification, a negligible reduction in rejection rates was observed in the first 72 h.

As mentioned above, we found that when the membrane was mechanically compressed and then thermally annealed, infinitesimally small reductions in rejection rates were observed even after 72 h of the membrane being in use. It has been widely mentioned in the literature that membranes undergo swelling and that physically controlling the pressure on a membrane can aid in controlling the *d*-spacing.[38] Additionally, membranes with stacked layers are anisotropic in nature and are capable of swelling only in the vertical direction, so applying external pressure and thermal annealing can greatly reduce the swelling, which is also evident from the observations.

The membrane's hydrophilicity impacts the water purification performance, as increasing the membrane's hydrophilicity will enhance the affinity for water molecules, which in turn allows for easier water passage and organic molecule rejection, leading to improved water flux. Thus, in this study, the membrane's hydrophilicity was assessed using a contact angle test, and the results are presented in Figure 5. The GO-MXene membrane before and after thermal annealing (v-GO-M and v-120-GO-M) showed water contact angles of 69.6, 64.2, and 63.5°, respectively, which suggests an increase in hydrophilicity with annealing. Additionally, the water contact angle trend for the membranes follows the same trend as for the roughness values. This indicates that the enhanced hydrophilicity of the annealed GO-M is a result of the combined effects of thermal annealing and mechanical compression. Moreover, the decreasing contact angle, as shown in Figure 5A(a−c), after

https://doi.org/10.1021/acsenvironau.3c00059
ACS Environ. Au 2024, 4, 69−79

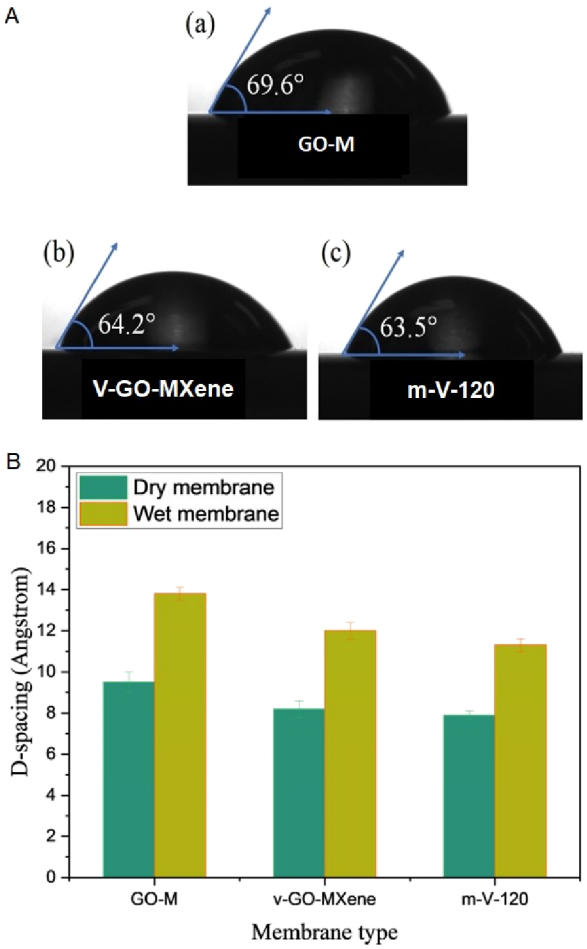

Figure 5. (A) Membrane surface contact angle measurements for (a) GO-M, (b) v-GO-MXene, and (c) m-v-120. (B) Interlayer *d*-spacing for dry and wet membranes.

thermal annealing is likely due to the dehydroxylation during self-cross-linking and carboxylate cross-linking between the neighboring MXene and GO nanosheets.

The dynamic cross-linking was also found to result in a suppressed *d*-spacing when compared to GO-MXene and mechanically compressed GO-MXene. Figure S12 shows the raw XRD data plots for the same. This interaction between the adjacent sheets causes a relatively fixed interlayer spacing in solutions, thereby suppressing the swelling behavior of the GO-M. The thermally annealed composite membrane (v-GO-M) exhibited a *d*-spacing of 12 Å in wet state and 8.2 Å in dry state (Figure 5B), and as a result, the composite membrane showed high rejection for salts and organic dyes. Next, the combination of mechanical compression and thermal annealing produced (m-v-120-GO-M) reduced *d*-spacing compared to the prior membranes. The *d*-spacing was 11.3 Å for wet and 7.9 Å for dry state, respectively (7.9 Å is the lowest *d*-spacing observed to date).[39] Here, the reduction in the *d*-spacing is profound for m-v-120-GO-M membrane samples. This reduction in interlayer *d*-spacing leads to improved salt rejection for both NaCl and $MgCl_2$. Additionally, using GO-M in one membrane reduces the chances of pinhole creation because the flake sizes of both GO and MXene are different, thereby eliminating the feed bypass. Thus, by using GO-M, we successfully prepared thermally annealed GO-M composite membranes that achieved the best interaction between GO-M and the highest salt rejection. As can be seen in Figure S12, the *d*-space of m-v-120-GO-M is almost equal to that of GO-M (i.e., even after intercalating MXene with GO membrane).

Permeation Measurement and Testing

We conducted permeation experiments to assess the effectiveness of the GO-Mxene membrane in rejecting NaCl, $MgCl_2$, and organics in water solutions. The filtration tests were carried out using a dead-end filtration apparatus (shown in Figure S13) pressurized with nitrogen gas at less than 2 bar. The composite membrane's rejection behavior for NaCl and $MgCl_2$ varied depending on their concentrations (500−5000 ppm). We observed higher rejection rates for larger organic molecules due to the clogging of the pores by those molecules, resulting in reduced diffusion (shown in Figure 6a). Additionally, the mechanical and thermal annealing of the GO-MXene layer increased the diffusion length of water, resulting in a lower water permeation for the composite membrane than the GO membrane.

This unique membrane microstructure annealing effect has a remarkable impact on the solute rejection. Figure 6B,C shows the NaCl and $MgCl_2$ rejection at different salt concentrations ranging from 500 to 5000 ppm. The trends show that thermal annealing improved the salt rejection to a greater extent when compared to mechanical compression and the pristine GO-MXene membrane. Also, it is important to note that lower rejection at higher salt concentrations may indicate that membrane charge is affecting salt rejection via Donnan exclusion[40−42] We have also tested organic rejection using these membranes wherein Allura red AC (496.42 g/mol), methyl blue (800 g/mol), and Victoria blue 4R (520.1 g/mol) were used. Here, we choose three different dyes based on their charge: Allura red is an acidic dye; Victoria blue 4R and methyl blue are basic dyes. Because methyl blue and Victoria blue 4R are large-sized molecules, their rejection remains higher (97−99.5%) irrespective of their charge. However, the Allura red AC is a small molecule with slightly lower rejection (88%). The feed and permeate streams, along with their UV−vis absorbance curves, are shown in Figure S15.

The pure water flux trend in the GO-MXene membranes has been observed to be in the order GO-M > v-GO-M > m-v-120. This trend is obvious because both v-GO-M and m-v-120 exhibit reduced d-spacing as compared to GO-M. Although the fluxes for salt solutions are somewhat lower primarily because of the higher concentration of total dissolved solids, the difference remains significantly smaller in comparison to the pure water flux.

GO and MXene have impressive adsorption capabilities for organic molecules, and to confirm the extent to which the m-v-120-GO-M contributed to the separation performance via organic adsorption, the authors performed the following control experiment. This experiment involved the utilization of the m-v-120-GO-M membrane under the dead-end mode of operation to assess the rejection of specific organic dyes, namely, Victoria blue, methyl blue, and Allure red AC, while maintaining a consistent dye content of 0.1 mg across all samples as shown in Figure S18. Here, the absorbance spectra of the retentate surpass those of the feed, primarily as a result of an increase in organic concentration occurring during the separation process. Following the experiment, a quantitative analysis was performed to determine the total quantity of dye present in both the permeate and the retentate (the sum of dye content available in the permeate and retentate after the

https://doi.org/10.1021/acsenvironau.3c00059
ACS Environ. Au 2024, 4, 69−79

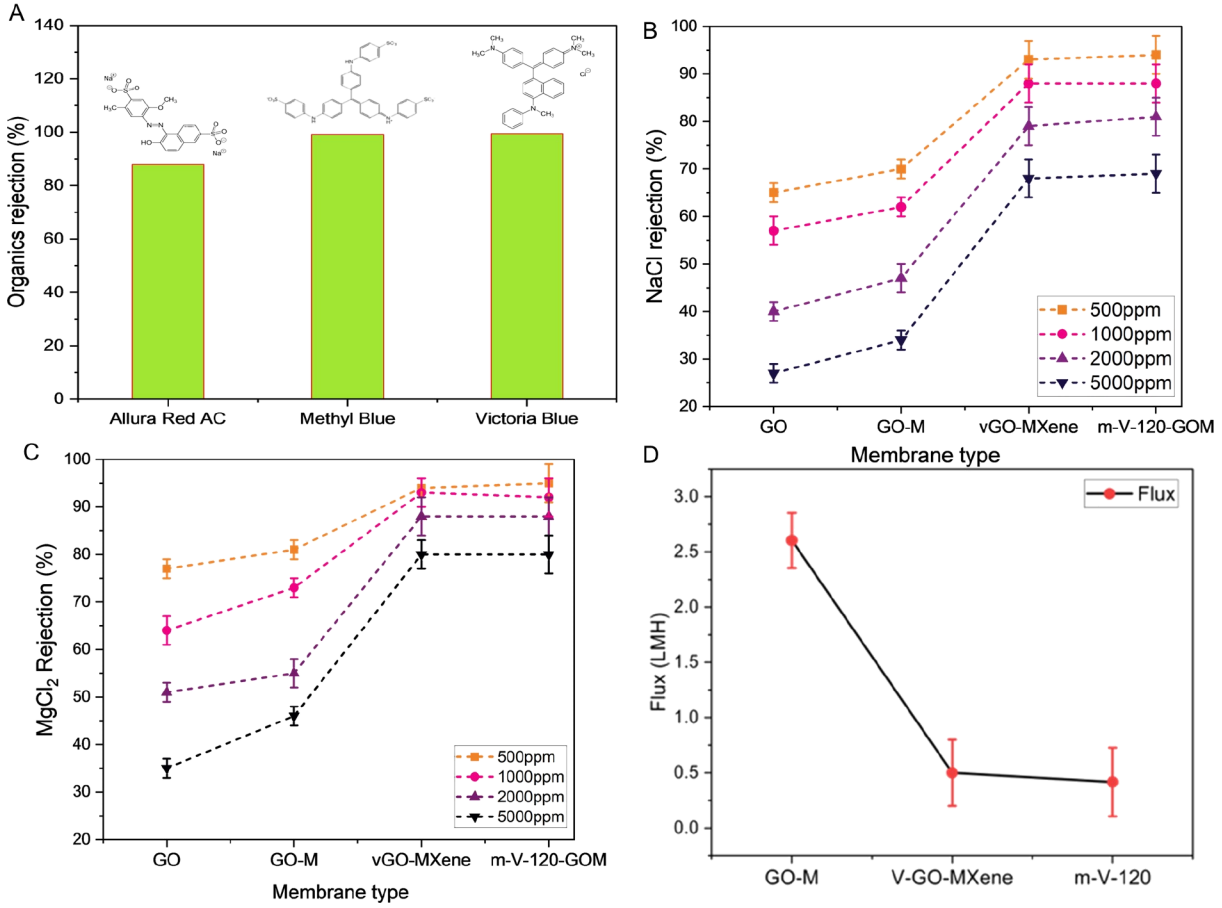

Figure 6. (a) The membrane organic rejection using Allura red AC, methyl blue, and Victoria blue 4R. Salt rejection for different GO-MXene membranes at varying salt concentrations for (b) NaCl and (c) $MgCl_2$. (d) Water flux for GO-M, v-GO-M, and m-v-120-GO-M membranes.

experiment). Remarkably, this analysis revealed that the quantity of organic dye in both the permeate and retentate equaled the initial 0.1 mg, indicating an absence of significant adsorption by the GO-MXene membrane. Had the adsorption occurred, the cumulative organic dye content in the permeate and retentate would have been lower than that in the initial feed solution, which was not the case here. Thus, adsorption makes no contribution to the membrane separation behavior in our study. The dye rejection trends were also examined over a period of 72 h. During the initial 48 h, there was a higher level of rejection compared to the period between 48 and 72 h. A decrease of 10−15% in the overall rejection was observed and is illustrated in detail in Figures S14−S17. The v-GO-MXene membranes encountered issues with delamination at low pressure, which was insufficient to counteract their swelling behavior. To address this, we devised a solution involving mechanical compression of the membranes followed by thermal annealing. This approach increased the exposed cross-linking area and reduced the interlayer *d*-spacing accordingly. Herein, the enhanced rejection effect is due to the decreased membraned *d*-spacing that occurs because of membrane dynamic cross-linking. In summary, the self- and carboxylate cross-linking introduced between the GO-MXene membrane creates a steric barrier for solute molecules to easily pass through them, thus elevating the rejection.

CONCLUSIONS

This study presents a novel approach for water purification by developing a GO-MXene composite membrane with hierarchical assembly, self-cross-linking, and carboxylate cross-linking abilities. In summary, to enhance the separation performance of GO membranes, a design strategy has been incorporated that involves making a tortuous 2D channel between the GO galleries by tailoring the interlayer *d*-spacing while incorporating MXene followed by mechanical compression and thermal annealing. Because MXene possesses smaller flakes, using it as an intercalating agent enhances the tortuosity of channel spaces and improves rejection. Within GO-MXene membranes, MXene acts as a spacer, creating adjustable subnanochannels between adjacent GO nanosheets and effectively functioning as molecular sieves that impede the passage of solutes with hydrated radii larger than the dimensions of these subnanochannels. Therefore, GO-MXene membranes demonstrate significant potential for applications in water purification, desalination, and molecular separation. The membrane exhibited a remarkable increase in the water flux and a high rejection of salt solutions, indicating its high efficiency for water purification. The exceptional performance is attributed to the thermal annealing process, which promotes the migration and rearrangement of GO-MXene flakes and creates dynamic cross-linking between GO and MXene. Additionally, thermal annealing increased the surface hydrophilicity of the membrane as it led to a reduction in water contact angles, leading to improved water adsorption and

https://doi.org/10.1021/acsenvironau.3c00059
ACS Environ. Au 2024, 4, 69−79

enhanced separation effect of channels. Furthermore, the GO-MXene membrane showed an impressive rejection property toward organic molecules as well due to their suppressed *d*-spacings after thermal annealing. The results of this study imply that the suggested approach (thermal annealing followed by mechanical compression) could be a potential solution for creating long-lasting and efficient membranes for water purification, creating covalent bonds instead of weak non-covalent interactions. Furthermore, this research could serve as a reference for the design of other innovative membranes in this area for larger-scale applications. Lastly, this work will open more avenues for future research, and one of these can be done by studying the effect of different intercalants such as hBN or other types of MXenes. Also, in this study, high rejection was observed for small salt ions, and thus, there remains a scope for theoretical studies aiming to explore a strong reason for this observation.

■ ASSOCIATED CONTENT

Supporting Information

The Supporting Information is available free of charge at https://pubs.acs.org/doi/10.1021/acsenvironau.3c00059.

Pictorial representation of different GO-MXene membranes; XRD spectra of MXene; size distribution of GO and MXene nanosheets; SEM cross-sectional view of the PES substrate; SEM images (top view and cross-sectional view) of GO-M and m-v-120-GO-M; FTIR spectra of GO-M and m-v-120-GO-M; XPS spectra for O 1s in GO-M and m-v-120 GO-M; AFM image of GO-M; XRD image of dry and wet GO-M, v-GO-M, and m-v-120-GO-M; pictorial representation of dye rejection membranes; UV−vis spectra of dyes; and rejection performance of recently published GO membranes (PDF)

■ AUTHOR INFORMATION

Corresponding Author

Alamgir Karim − *Department of Chemical and Biomolecular Engineering, University of Houston, Houston, Texas 77204, United States;* orcid.org/0000-0003-1302-9374; Email: akarim3@central.uh.edu

Authors

Saurabh Kr Tiwary − *Department of Chemical and Biomolecular Engineering, University of Houston, Houston, Texas 77204, United States;* orcid.org/0000-0003-2255-7443

Maninderjeet Singh − *Department of Chemical and Biomolecular Engineering, University of Houston, Houston, Texas 77204, United States;* orcid.org/0000-0001-8891-8454

Farzana Hasan Likhi − *Department of Material Science and Engineering, University of Houston, Houston, Texas 77204, United States*

Siddharaj Dabade − *Department of Chemical and Biomolecular Engineering, University of Houston, Houston, Texas 77204, United States*

Jack F. Douglas − *Material Science and Engineering Division, National Institute of Standards and Technology, Gaithersburg, Maryland 20899, United States;* orcid.org/0000-0001-7290-2300

Complete contact information is available at: https://pubs.acs.org/10.1021/acsenvironau.3c00059

Author Contributions

CRediT: **Saurabh Kr Tiwary** conceptualization, investigation, data curation, project administration, foraml analysis, writing;- **Maninderjeet Singh** conceptualization, investigation, project administration, resources, validation, writing-review & editing; **Farzana Hasan Likhi** data curation, methodology, resources, software; **Siddharaj Dabade** conceptualization, data curation, formal analysis, methodology, validation, visualization, writing-original draft; **Jack F. Douglas** visualization, writing-review & editing; **Alamgir Karim** conceptualization, funding acquisition, investigation, project administration, supervision, visualization, writing-review & editing.

Notes

The authors declare no competing financial interest.

Certain commercial equipment, instruments, or materials are identified in this paper to specify the experimental procedure accurately. Such identification is not intended to imply recommendation or endorsement by the National Institute of Standards and Technology, nor is it intended to imply that the equipment or materials identified are necessarily the best available for the purpose.

■ ACKNOWLEDGMENTS

The authors acknowledge funding from NSF DMR # 1900692, ACS PRF # 66838-ND7, WELCH # E-2105-20220331 and WELCH # V-E-0003-20230731 grants for the design of experiments, data interpretation, sample fabrication, measurements, and characterization aspects of this work. Also, we thank Dr. Devin L. Shaffer of the University of Houston for his valuable feedback.

■ REFERENCES

(1) Griggs, C. S.; Medina, V. F. Graphene and Graphene Oxide Membranes for Water Treatment. *McGraw Hill Encyclopedia Sci. Technol.* **2016**, DOI: 10.1036/1097-8542.YB150695.

(2) Liu, Y. IOP Conference Series: Earth and Environmental Science Application of Graphene Oxide in Water Treatment Mechanical Properties of Two-Dimensional Materials and Their Applications Two-Dimensional Materials for Novel Liquid Separation Membranes Application of Graphene Oxide in Water Treatment. *IOP Conf. Ser. Earth Environ. Sci.* **2017**, *94*, No. 012060, DOI: 10.1088/1755-1315/94/1/012060.

(3) Sharif, S.; Ahmad, K. S.; Rehman, F.; Bhatti, Z.; Thebo, K. H. Two-Dimensional Graphene Oxide Based Membranes for Ionic and Molecular Separation: Current Status and Challenges. *J. Environ. Chem. Eng.* **2021**, *9* (4), No. 105605.

(4) An, Y. C.; Gao, X. X.; Jiang, W. L.; Han, J. L.; Ye, Y.; Chen, T. M.; Ren, R. Y.; Zhang, J. H.; Liang, B.; Li, Z. L.; Wang, A. J.; Ren, N. Q. A Critical Review on Graphene Oxide Membrane for Industrial Wastewater Treatment. *Environ. Res.* **2023**, *223*, No. 115409.

(5) Wang, X.; Zhao, Y.; Tian, E.; Li, J.; Ren, Y. Graphene Oxide-Based Polymeric Membranes for Water Treatment. *Adv. Mater. Interfaces* **2018**, *5* (15), 1701427.

(6) Gong, D.; Liu, X.; Wu, P.; Wang, Y.; Guo, B.; Liu, S.; Chen, H.; Yin, Y.; Liu, G.; Liu, M.; Miao, Q.; Yu, C.; Fan, J.; Li, Z.; Shi, G.; Sun, Y.; He, Y.; Zeng, G. Water Pumping Effect over the Organic Ions Defined Graphene Oxide Membrane Impulses High Flux Desalination. *npj Clean Water* **2022**, *5* (1), 1−9.

(7) Ghobadi Moghadam, A.; Hemmati, A. Improved Water Purification by PVDF Ultrafiltration Membrane Modified with GO-PVA-NaAlg Hydrogel. *Sci. Rep.* **2023**, *13* (1), 1−16.

(8) Chen, D.; Feng, H.; Li, J. Graphene Oxide: Preparation, Functionalization, and Electrochemical Applications. *Chem. Rev.* **2012**, *112* (11), 6027−6053.
(9) Yang, C.; Long, M.; Ding, C.; Zhang, R.; Zhang, S.; Yuan, J.; Zhi, K.; Yin, Z.; Zheng, Y.; Liu, Y.; Wu, H.; Jiang, Z. Antifouling Graphene Oxide Membranes for Oil-Water Separation via Hydrophobic Chain Engineering. *Nat. Commun.* **2022**, *13* (1), 1−9.
(10) Seo, D. H.; Pineda, S.; Woo, Y. C.; Xie, M.; Murdock, A. T.; Ang, E. Y. M.; Jiao, Y.; Park, M. J.; Lim, S. Il; Lawn, M.; Borghi, F. F.; Han, Z. J.; Gray, S.; Millar, G.; Du, A.; Shon, H. K.; Ng, T. Y.; Ostrikov, K. Anti-Fouling Graphene-Based Membranes for Effective Water Desalination. *Nat. Commun.* **2018**, *9* (1), 1−12.
(11) Janjhi, F. A.; Janwery, D.; Chandio, I.; Ullah, S.; Rehman, F.; Memon, A. A.; Hakami, J.; Khan, F.; Boczkaj, G.; Thebo, K. H. Recent Advances in Graphene Oxide-Based Membranes for Heavy Metal Ions Separation. *ChemBioEng. Reviews* **2022**, *9* (6), 574−590.
(12) Jatoi, A. H.; Kim, K. H.; Khan, M. A.; Memon, F. H.; Iqbal, M.; Janwery, D.; Phulpoto, S. N.; Samantasinghar, A.; Choi, K. H.; Thebo, K. H. Functionalized Graphene Oxide-Based Lamellar Membranes for Organic Solvent Nanofiltration Applications. *RSC Adv.* **2023**, *13*, 12695−12702.
(13) Jee, H.; Jang, J.; Kang, Y.; Eisa, T.; Chae, K. J.; Kim, I. S.; Yang, E. Enhancing the Dye-Rejection Efficiencies and Stability of Graphene Oxide-Based Nanofiltration Membranes via Divalent Cation Intercalation and Mild Reduction. *Membranes* **2022**, *12* (4), 402.
(14) Chandio, I.; Janjhi, F. A.; Memon, A. A.; Memon, S.; Ali, Z.; Thebo, K. H.; Pirzado, A. A. A.; Hakro, A. A.; Khan, W. S. Ultrafast Ionic and Molecular Sieving through Graphene Oxide Based Composite Membranes. *Desalination* **2021**, *500*, No. 114848.
(15) Chen, L.; Shi, G.; Shen, J.; Peng, B.; Zhang, B.; Wang, Y.; Bian, F.; Wang, J.; Li, D.; Qian, Z.; Xu, G.; Liu, G.; Zeng, J.; Zhang, L.; Yang, Y.; Zhou, G.; Wu, M.; Jin, W.; Li, J.; Fang, H. Ion Sieving in Graphene Oxide Membranes via Cationic Control of Interlayer Spacing. *Nature* **2017**, *550*, 380−383.
(16) Kang, K. M.; Kim, D. W.; Ren, C. E.; Cho, K. M.; Kim, S. J.; Choi, J. H.; Nam, Y. T.; Gogotsi, Y.; Jung, H. T. Selective Molecular Separation on Ti3C2Tx-Graphene Oxide Membranes during Pressure-Driven Filtration: Comparison with Graphene Oxide and MXenes. *ACS Appl. Mater. Interfaces* **2017**, *9* (51), 44687−44694.
(17) Lu, Z.; Wei, Y.; Deng, J.; Ding, L.; Li, Z. K.; Wang, H. Correction to "Self-Crosslinked MXene (Ti3C2Tx) Membranes with Good Antiswelling Property for Monovalent Metal Ion Exclusion. *ACS Nano* **2023**, *13* (9), 12934.
(18) Homaeigohar, S.; Elbahri, M. Graphene Membranes for Water Desalination. *NPG Asia Materials* **2017**, *9* (8), e427−e427.
(19) Li, Z.; Dai, J.; Li, Y.; Sun, C.; Meng, A.; Cheng, R.; Zhao, J.; Hu, M.; Wang, X. Intercalation-Deintercalation Design in MXenes for High-Performance Supercapacitors. *Nano Res.* **2022**, *15* (4), 3213−3221.
(20) Li, Y.; Huang, S.; Wei, C.; Wu, C.; Mochalin, V. N. Adhesion of Two-Dimensional Titanium Carbides (MXenes) and Graphene to Silicon. *Nature Communications* **2019**, *10* (1), 1−8.
(21) Yang, J.; Naguib, M.; Ghidiu, M.; Pan, L. M.; Gu, J.; Nanda, J.; Halim, J.; Gogotsi, Y.; Barsoum, M. W. Two-Dimensional Nb-Based M 4 C 3 Solid Solutions (MXenes). *J. Am. Ceram. Soc.* **2016**, *99* (2), 660−666.
(22) Bera, S.; Singh, M.; Thantirige, R.; Tiwary, S. K.; Shook, B. T.; Nieves, E.; Raghavan, D.; Karim, A.; Pradhan, N. R. 2D-Nanofiller-Based Polymer Nanocomposites for Capacitive Energy Storage Applications. *Small Science* **2023**, *3* (7), 2300016.
(23) Singh, M.; Das, P.; Samanta, P. N.; Bera, S.; Thantirige, R.; Shook, B.; Nejat, R.; Behera, B.; Zhang, Q.; Dai, Q.; Pramanik, A.; Ray, P.; Raghavan, D.; Leszczynski, J.; Karim, A.; Pradhan, N. R. Ultrahigh Capacitive Energy Density in Stratified 2D Nanofiller-Based Polymer Dielectric Films. *ACS Nano* **2023**, *17* (20), 20262−20272.
(24) Naguib, M.; Mochalin, V. N.; Barsoum, M. W.; Gogotsi, Y. 25th Anniversary Article: MXenes: A New Family of Two-Dimensional Materials. *Adv. Mater.* **2014**, *26* (7), 992−1005.
(25) Xin, M.; Li, J.; Ma, Z.; Pan, L.; Shi, Y. MXenes and Their Applications in Wearable Sensors. *Front Chem.* **2020**, *8*, 297.
(26) Huang, H.; Park, H.; Huang, J. Self-Crosslinking of Graphene Oxide Sheets by Dehydration Highlights GO Sheets Can. Covalently Self-Crosslink upon Dehydration Dehydration Triggers Esterification between Neighboring Sheets Self-Crosslinking Greatly Alters the Processability of GO Materials Self-Crosslinking of Graphene Oxide Sheets by Dehydration. *Chem.* **2022**, *8* (9), 2432−2441.
(27) Lu, Z.; Wei, Y.; Deng, J.; Ding, L.; Li, Z. K.; Wang, H. Erratum: Self-Crosslinked MXene (Ti3C2Tx) Membranes with Good Anti-swelling Property for Monovalent Metal Ion Exclusion (ACS Nano (2019) 13:9 (10535−10544) DOI: 10.1021/Acsnano.9b04612). *ACS Nano* **2019**, *17* (13), 10535.
(28) Ta, Q. T. H.; Tran, N. M.; Noh, J. S. Rice Crust-Like ZnO/Ti 3 C 2 T x MXene Hybrid Structures for Improved Photocatalytic Activity. *Catalysts* **2020**, *10* (10), 1140.
(29) Shen, X.; Lin, X.; Yousefi, N.; Jia, J.; Kim, J. K. Wrinkling in Graphene Sheets and Graphene Oxide Papers. *Carbon N Y* **2014**, *66*, 84−92.
(30) Deng, S.; Berry, V. Wrinkled, Rippled and Crumpled Graphene: An Overview of Formation Mechanism, Electronic Properties, and Applications. *Mater. Today* **2016**, *19* (4), 197−212.
(31) An, Y. C.; Gao, X. X.; Jiang, W. L.; Han, J. L.; Ye, Y.; Chen, T. M.; Ren, R. Y.; Zhang, J. H.; Liang, B.; Li, Z. L.; Wang, A. J.; Ren, N. Q. A Critical Review on Graphene Oxide Membrane for Industrial Wastewater Treatment. *Environ. Res.* **2023**, *223*, No. 115409.
(32) Li, Y.; Huang, S.; Wei, C.; Wu, C.; Mochalin, V. N. Adhesion of Two-Dimensional Titanium Carbides (MXenes) and Graphene to Silicon. *Nature Communications 2019 10:1* **2019**, *10* (1), 1−8.
(33) Liu, T.; Zhang, X.; Liang, J.; Liang, W.; Qi, W.; Tian, L.; Qian, L.; Li, Z.; Chen, X. Ultraflat Graphene Oxide Membranes with Newton-Ring Prepared by Vortex Shear Field for Ion Sieving. *Nano Lett.* **2023**, 9641 DOI: 10.1021/ACS.NANOLETT.3C02613/SUPPL_FILE/NL3C02613_SI_001.PDF.
(34) Willcox, J. A. L.; Kim, H. J. Molecular Dynamics Study of Water Flow across Multiple Layers of Pristine, Oxidized, and Mixed Regions of Graphene Oxide. *ACS Nano* **2017**, *11* (2), 2187−2193.
(35) Wei, N.; Peng, X.; Xu, Z. Understanding Water Permeation in Graphene Oxide Membranes. *ACS Appl. Mater. Interfaces* **2014**, *6* (8), 5877−5883.
(36) Jiao, S.; Xu, Z. Non-Continuum Intercalated Water Diffusion Explains Fast Permeation through Graphene Oxide Membranes. *ACS Nano* **2017**, *11* (11), 11152−11161.
(37) Adstedt, K.; Buxton, M. L.; Henderson, L. C.; Hayne, D. J.; Nepal, D.; Gogotsi, Y.; Tsukruk, V. V. 2D Graphene Oxide and MXene Nanosheets at Carbon Fiber Surfaces. *Carbon N Y* **2023**, *203*, 161−171.
(38) Wang, Z.; Ma, C.; Xu, C.; Sinquefield, S. A.; Shofner, M. L.; Nair, S. Graphene Oxide Nanofiltration Membranes for Desalination under Realistic Conditions. *Nat. Sustain* **2021**, *4*, 402−408.
(39) Adstedt, K.; Buxton, M. L.; Henderson, L. C.; Hayne, D. J.; Nepal, D.; Gogotsi, Y.; Tsukruk, V. V. 2D Graphene Oxide and MXene Nanosheets at Carbon Fiber Surfaces. *Carbon N Y* **2023**, *203*, 161−171.
(40) Aher, A.; Nickerson, T.; Jordan, C.; Thorpe, F.; Hatakeyama, E.; Ormsbee, L.; Majumder, M.; Bhattacharyya, D. Ion and Organic Transport in Graphene Oxide Membranes: Model Development to Difficult Water Remediation Applications. *J. Membr. Sci.* **2020**, *604*, No. 118024.
(41) Liu, G.; Ye, H.; Li, A.; Zhu, C.; Jiang, H.; Liu, Y.; Han, K.; Zhou, Y. Graphene Oxide for High-Efficiency Separation Membranes: Role of Electrostatic Interactions. *Carbon* **2016**, *110*, 56−61.
(42) Hu, C.; Liu, Z.; Lu, X.; Sun, J.; Liu, H.; Qu, J. Enhancement of the Donnan Effect through Capacitive Ion Increase Using an Electroconductive RGO-CNT Nanofiltration Membrane †. *J. Mater. Chem. A* **2018**, *6*, 4737−4745.